Microscopic mechanisms behind hyperferroelectricity

Mohamed Khedidji,[1] Danila Amoroso,[2] and Hania Djani[3]
[1]*Laboratoire CTCP, Université des Sciences et de la Technologie Houari Boumedienne, B.P.32, El Alia, Bab Ezzouar, Alger, Algeria*
[2]*National Research Council CNR-SPIN, c/o Università degli Studi "G. D'Annunzio", I-66100 Chieti, Italy*
[3]*Centre de Développement des Technologies Avancées, Cité 20 août 1956, Baba Hassen, Alger, Algeria*

(Received 2 November 2020; accepted 7 January 2021; published 26 January 2021)

Hyperferroelectrics are observing a growing interest thanks to their unique property to retain a spontaneous polarization even in the presence of a depolarizing field, corresponding to zero macroscopic displacement field ($\mathbf{D} = 0$) conditions. Hyperferroelectricity is ascribed to the softening of a polar *LO* mode, but the microscopic mechanisms behind this softening are not totally resolved. Here, by means of phonon calculations and force constants analysis, performed in two classes of hyperferroelectrics, the ABO_3-LiNbO3-type systems and the hexagonal-ABC systems, we unveil the common features in the dynamical properties of a hyperferroelectric that lead the *LO* instability: negative or vanishing on-site force constant associated to the cation driving the *LO* polar mode and a destabilizing cation-anion interaction; both induced by short-range forces. We also predict a possible enhancement of the hyperferroelectric properties under increasing external positive pressures: pressure strengthens the destabilizing short-range interactions, inducing a stronger *LO* mode instability and the increase of the longitudinal mode effective charges associated to the unstable *LO* mode. This suggests an eventual enhancement of the $\mathbf{D} = 0$ polarization under compressive strain.

DOI: 10.1103/PhysRevB.103.014116

I. INTRODUCTION

The concept of *hyperferroelectricity* (hyperFE) was first introduced in semiconducting hexagonal ABC ferroelectrics (FE) by Garrity *et al.* in Ref. [1]. The prefix *hyper* is related to the intrinsic property of such a new class of proper ferroelectrics to display a persistent polarization even in the presence of a depolarization field; something unachievable by standard ferroelectrics (FE) [1,2]. In fact, by analyzing the electric equation of state, Garrity *et al.* showed that, in contrast to standard ferroelectrics, which spontaneously polarize only under zero macroscopic electric field ($\mathbf{E} = 0$), hyperferroelectrics can spontaneously polarize under both zero macroscopic electric field ($\mathbf{E} = 0$) and zero macroscopic displacement field ($\mathbf{D} = 0$), i.e., unscreened depolarization field under open circuit boundary conditions. Such features thus make hyperFE systems suitable for applications as low-dimensional functional materials [3–7]; moreover, the existence of a switchable electric polarization in hyperFEs can be allowed in metals and not restricted to only insulators and semiconductors as for standard FEs [4,8,9].

The difference in behavior between FE and hyperFE systems stems from the different type of lattice instabilities displayed in the paraelectric phase, as it was first pointed out by Garrity *et al.*: the well-known FE instability is related to an unstable zone-center transverse optic (TO) mode [10,11]; the hyperFE instability is related to an unstable zone-center longitudinal optic (LO) mode beside the unstable TO one. Moreover, they ascribed the appearance of such unstable LO mode in the narrow-gap ABC hyperFEs, to a small LO-TO splitting resulting from the small Born effective charges (BEC) and relatively large electronic contribution to the dielectric constant ϵ^{∞} [12]. Nevertheless, in a later work, Li *et al.* [9] reported unstable LO modes also in some $LiNbO_3$-type ferroelectrics showing, on the contrary, anomalous BEC and small ϵ^{∞}. This apparent contradiction motivated these authors to provide a further insight into the microscopic mechanisms behind the LO mode instability. By modeling the $LiNbO_3$-type systems via an effective Hamiltonian, they identified the structural instabilities related to Li atoms, driven by short-range interactions, as the origin of the hyperferroelectricity. Nonetheless, the identification of the common microscopic origin behind the softening of this LO mode is still under debate.

In this work, by means of density functional theory (DFT) calculations and the analysis of the dynamical properties calculated employing density functional perturbation theory (DFPT), we confirm and discuss in detail the direct relationship between the unstable LO mode and destabilizing short-range (SR) interactions in ABO_3-$LiNbO_3$-type oxides (with A = Li,Na and B = Ta,Nb,V). Furthermore, we extend our findings to the hexagonal ABC systems: LiBeSb, LiZnP, LiZnAs, and NaMgP compounds, as representative examples. In particular, the exploration of the real-space on-site and interatomic force constants (IFCs) allowed us to distinguish between specific contributions of the long-range (LR) and short-range (SR) forces to the interatomic interactions that are, in turn, related to the structural properties of the investigated systems. Our study reveals common microscopic mechanisms driving hyperferroelectricity: a structural frustration, arising from the undercoordination of the small-sized A atom in $LiNbO_3$-type systems and small-sized B atom in the

hexagonal ABC, induces the off-centering of the frustrated cations towards the neighboring out-of-plane anions. Such polar distortion is not only driven by LR dipole-dipole interactions but also by SR interactions; the first one contributing to the ferroelectric (TO mode) instability and the second to the hyperferroelectric (LO mode) one. Additionally, we also investigated the effect of external isotropic pressure on the $LiNbO_3$-type systems, finding out a possible enhancement of hyperferroelectricity.

II. METHODS

Calculations were performed within DFT [13,14] using a plane waves method as implemented in the ABINIT package [15]. The exchange correlation energy functional was evaluated within the generalized gradient approximation (GGA) employing the revised Perdew-Burke-Ernzerhof functional PBEsol [16,17]. The wave functions were expanded up to a kinetic energy cutoff of 45 Hartrees. Integrals over the Brillouin zone were approximated by sums on a a $6 \times 6 \times 6$ Monkhorst-Pack k-points mesh [18]. We relaxed the structure until the remaining forces on the atoms were less than 10^{-5} Hartree/Bohr and the stresses on the unit cell smaller than 10^{-7}. Phonons frequencies, IFCs, Born effective charges, and dielectric tensors were computed on the primitive paraelectric $R\bar{3}c$ phase using density-functional perturbation theory (DFPT) [19,20]. Note that the high temperature paraelectric $R\bar{3}c$ phase is experimentally observed for $LiTaO_3$ and $LiNbO_3$ and hypothetical for $LiVO_3$ and $NaVO_3$, but considered here to analyze trends and understand mechanisms. We also performed relaxation and DFPT calculations on hexagonal ABC systems in the paraelectric cubic $P6_3/mmc$ phase, using the GGA-PBEsol functional, with a $6 \times 6 \times 6$ Monkhorst-Pack mesh and a kinetic energy cutoff of 45 Hartrees.

III. RESULTS

In order to provide a clear understanding of mechanisms at play in hyperFEs, we proceeded step-by-step: first, we presented the structural properties of $LiTaO_3$, $LiNbO_3$, $LiVO_3$, and $NaVO_3$ in the centrosymmetric paraelectric $R\bar{3}c$ phase and their relationship with the associated low-symmetry polar $R3c$ phase. Then, we discussed the dynamical properties of the paraelectric phase. In particular, we reported phonons modes at the Γ-point, with a special focus on phonons associated to polar displacements along the cartesian z-direction (corresponding to the $R\bar{3}c$ trigonal axis) that are driving the observed ferroelectric phase transition in $LiTaO_3$ and $LiNbO_3$. Phonons frequencies, eigendisplacements, and mode effective charges are reported, together with the real space on-site and interatomic force constants, that are of particular importance here to reveal the interatomic interactions behind the softening of the LO mode.

A. Structural properties

In ABO_3-$LiNbO_3$-type oxides, the paraelectric structure of $R\bar{3}c$ symmetry (Fig. 1) counts ten atoms in its rhombohedral primitive cell (or 30 atoms in the hexagonal conventional cell) (see Ref. [21]). The atomic arrangement consists of chains of equidistant A-site (Li, Na) and B-site (Ta, Nb, V)

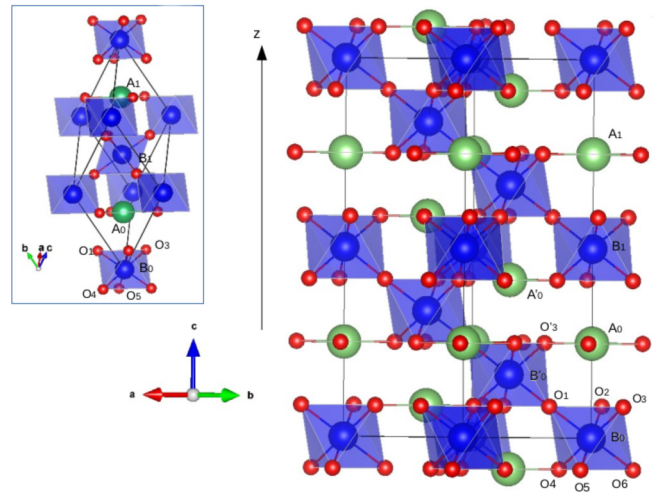

FIG. 1. The paraelectric $R\bar{3}c$ structure of ABO_3-$LiNbO_3$-type oxides in its conventional hexagonal unit cell (the primitive rhombohedral unit cell inset). A atoms are in green color, B atoms in blue, and O atoms in red.

atoms along the trigonal axis (Cartesian z-direction). As illustrated in Fig. 1, the transition-metal B atoms occupy the center of oxygen octahedra and the A atoms sit at the center of the in-plane nearest neighbors O-triangle and have six further next near neighbors out-of-plane oxygens (out-of-plane $O_{1,2,3}$, equivalent to $O_{4,5,6}$) [see also Fig. 2(a)]. The ferroelectric structure of $R3c$ symmetry originates from the off-centering of B and A atoms along the trigonal axis [see Fig. 2(b)]. In particular, the Li-O polar displacement tends to improve the Li coordination environment by coming closer to three of the six out-of-plane oxygens (Li-O_1) and moving

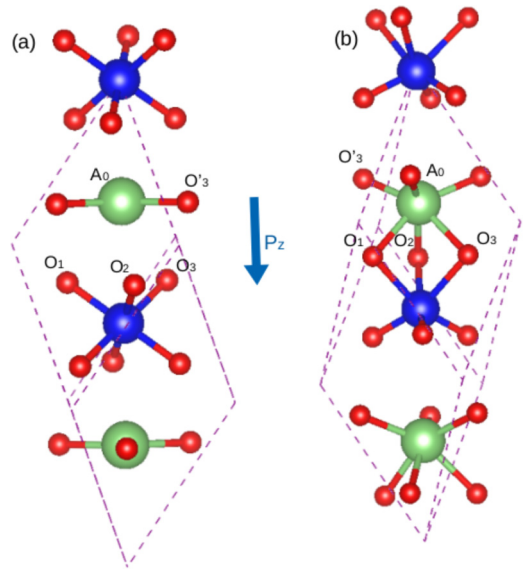

FIG. 2. (a) In the paraelectric $R\bar{3}c$ phase, Li is undercoordinated (surrounded with three in-plane oxygens). (b) In the ferroelectric $R3c$, Li displaces toward the out-of-plane oxygens cage along the z-direction, optimizing its coordination from III to VI.

TABLE I. Distances of Li-O bonds (Å) in the paraelectric $R\bar{3}c$ and ferroelectric $R3c$ phases. During the ferroelectric $R\bar{3}c$ to $R3c$ transition, A atoms move away from O'_3 (the A_0-O'_3 distances increase) and get closer to O_1 (the A_0-O_1 distances decrease).

	$LiTaO_3$		$LiNbO_3$		$LiVO_3$		$NaVO_3$	
Bond	Para	Ferro	Para	Ferro	Para	Ferro	Para	Ferro
A_0-O'_3	1.97	2.04	1.96	2.04	1.96	2.04	2.39	2.40
A_0-O_1	2.79	2.28	2.79	2.28	2.61	2.14	2.62	2.46

away from the three in-plane oxygens (Li-O'_3), as reported in Table I.

B. Phonon properties at Γ and interatomic force constants

Within the harmonic approximation, structural instabilities are associated to negative curvature of the internal energy with respect to specific atomic displacements, yielding imaginary phonon frequencies [25–27]. In line with the *"soft-mode theory"* first introduced by Cochran [28], the ferroelectric transition is ascribed to an unstable zone-center transverse optic (TO) phonon in the parent paraelectric phase associated to a polar atomic pattern of distortion; such a "ferroelectric" instability results from the delicate competition between stabilizing short-range (SR) forces and destabilizing long-range (LR) Coulomb interaction taking the form of a dipole-dipole (DD) interaction. In the following, we show that the "hyperferroelectricity" is rather resulting from an unstable zone-center longitudinal optic (LO) phonon driven by destabilizing SR forces.

Within the DPFT approach, the calculation of the interatomic force constants (IFCs), $C_{\alpha,\beta}(lk, l'k')$, and the analysis of the distinct SR and LR contributions, as defined in Ref. [29], allow to identify which driving forces lead the system to exhibit eventual instabilities [30,31]. In particular, within the used convention, the IFCs relates the α-component of the force $F_\alpha(lk)$ on atom k in cell l, to the induced displacement $\tau_\beta(l'k')$ of atom k' in cell l', through the expression $F_\alpha(lk) = -C_{\alpha,\beta}(lk, l'k')\tau_\beta(l'k')$ [30]: if the induced force on atom k is opposite to the direction of the displacement of atom k', a discordant cooperative atomic motion takes place, eventually producing break of the spatial inversion symmetry and so the creation of a dipole moment; accordingly, the IFC is positive and corresponds to a destabilizing interaction. Differently, the force on a single atom induced by its isolated displacement from its initial crystalline position is specified by the "on-site" force constant; this can be written as a sum over IFCs: $C_{\alpha,\beta}(lk, lk) = -\sum'_{l'k'} C_{\alpha,\beta}(lk, l'k')$ [30]. In this case, a negative on-site force constant means an instability against isolated atomic displacement: the induced force and the atomic displacement are concordant, favoring thus the off-centering from the initial position; at opposite, a positive value means stability against isolated atomic displacements, as the induced force will bring the atom back to its initial position. Accordingly, we reported in what follow the phonon properties at Γ-point and the interatomic force constants calculated in the primitive cell of the paraelectric $R\bar{3}c$ phase of $LiTaO_3$, $LiNbO_3$, $LiVO_3$, and $NaVO_3$.

TABLE II. Unstable modes at Γ in the paraelectric $R\bar{3}c$ phase. Γ_2^- is polar along the z-direction (trigonal axis), Γ_2^+ is antipolar along the z-direction, Γ_3^- is polar and doubly degenerated along xy-direction and Γ_3^+ is antipolar and doubly degenerated along the xy-direction. Our results are in agreements with previous works [9,22–24].

Mode irreps	$LiTaO_3$	$LiNbO_3$	$LiVO_3$	$NaVO_3$
Γ_2^- (A_{2u})	$164i$	$200i$	$448i$, $137i$	$459i$
Γ_2^+ (A_{2g})	$96i$	$102i$	$101i$	–
Γ_3^- (E_u)	–	$95i$	$386i$	$442i$
Γ_3^+ (E_g)	–	–	–	$279i$, $7i$

Several unstable transverse optic (TO) phonon modes are revealed at Γ (Table II), in agreement with previous DFT calculations [9,22–24]. For $LiTaO_3$, there is one polar mode Γ_2^- (A_{2u}) and one antipolar mode Γ_2^+ (A_{2g}) at higher frequency. For $LiNbO_3$, in addition to Γ_2^- and Γ_2^+ modes, there is Γ_3^- (E_u) polar mode at higher frequency, doubly degenerated in the xy-direction. For $LiVO_3$, there are two Γ_2^- modes, one Γ_2^+ and one doubly degenerate Γ_3^- mode. For $NaVO_3$ there is one Γ_2^- mode, one Γ_3^- mode and two antipolar Γ_3^+ (E_g) doubly degenerated in the xy-direction. It is worth noting that in $LiVO_3$ and $NaVO_3$, the modes are highly unstable compared to $LiTaO_3$ and $LiNbO_3$. Beside these unstable TO modes, we also found one unstable polar $LO1$ mode of Γ_2^- symmetry for $LiTaO_3$, $LiNbO_3$ and $LiVO_3$ ($\omega_{LO1} = 28i$ cm^{-1}, $77i$ and $138i$, respectively). Such $LO1$ mode is highly stable in $NaVO_3$ ($\omega_{LO1} = 154$ cm^{-1}).

In Table III, we report the eigendisplacements along the z-direction of the Γ_2^--TO modes (labeled $TO1$, $TO2$, and $TO3$) and $LO1$ mode, together with their associated frequencies. Mode effective charges $\bar{Z}^*_m$ are also reported: the α-component of the mode effective charge vector is defined as $\bar{Z}^*_{m,\alpha} = \frac{\sum_{k\beta} Z^*_{k,\alpha\beta}\eta_{m\boldsymbol{q}=0}(k\beta)}{[\sum_{k\beta}\eta^*_{m\boldsymbol{q}=0}(k\beta)\eta_{m\boldsymbol{q}=0}(k\beta)]^{1/2}}$ [20], where $\eta_{m\boldsymbol{q}=0}$ is the eigendisplacement associated to the mode m at the Γ-point and $Z^*_{k,\alpha\beta}$ are the Born effective charges -or transverse charges $\boldsymbol{Z}^{*(T)}$- for the TO-modes, and the Callen effective charges -or longitudinal charges $\boldsymbol{Z}^{*(L)}$- for the LO-modes; $\boldsymbol{Z}^{*(L)}$ is directly related to the $\boldsymbol{Z}^{*(T)}$ via the electronic dielectric tensor $\boldsymbol{\epsilon}_\infty$, i.e. $\boldsymbol{Z}^{*(L)}_k = \boldsymbol{\epsilon}_\infty^{-1}\boldsymbol{Z}^{*(T)}_k$ [32,33]. Complete $\boldsymbol{Z}^{*(T)}$ tensor and $\eta_{m\boldsymbol{q}=0}$ components are reported in the Supplemental Material (see Ref. [21]).

The eigendisplacements associated to the unstable $TO1$ modes show that A- and B-sites cations displace in phase along the trigonal axis, but in antiphase with respect to the oxygens. These modes exhibit a large mode effective charge, mostly resulting from the anomalous Born effective charges on the B atoms and oxygens (A atoms show values close to their nominal ionic charge), as reported in Table IV. In particular, a very large displacement of Li atoms characterizes $TO1$ in $LiTaO_3$ and $LiNbO_3$, in contrast to $LiVO_3$ and $NaVO_3$, where it is the V atoms at the B-site that move the most. In the latter compounds, the dominant B-site motion in $TO1$, combined with the very anomalous BEC on V and O atoms, produce the extremely large $\bar{Z}^*_{TO1}$ observed in $LiVO_3$ and $NaVO_3$ compared to $LiTaO_3$ and $LiNbO_3$. The eigendisplacements

TABLE III. Calculated phonon frequencies ω (cm^{-1}) of Γ_2^- TO- and $LO1$- modes with their corresponding normalized eigendisplacements (in a.u.) and mode effective charges $\bar{Z}_m^*$. The Callen longitudinal mode effective charge ($\bar{Z}_{LO1}^{*L}$) for $LO1$ is given between parenthesis. Decomposition of the phonon frequency into the LR and SR contributions is also reported ($\omega^2 = \omega_{\rm LR}^2 + \omega_{\rm SR}^2$).

	Modes	ω	A	B	$O_{1/2/3}$	$\bar{Z}_m^*$	ω^2	$\omega_{\rm LR}^2$	$\omega_{\rm SR}^2$
$LiTaO_3$	$TO1$	[164i]	+0.2081	+0.0080	−0.0605	4.64	−27056	+29634	−56690
	$TO2$	[149]	+0.1611	−0.0239	+0.0669	−4.42	+22203	−171327	+193531
	$TO3$	[512]	+0.0254	+0.0022	−0.0120	6.47	+262540	−581901	+844442
	$LO1$	[28i]	+0.2594	−0.0105	+0.0021	(0.077)	–	–	–
$LiNbO_3$	$TO1$	[201i]	+0.1544	+0.0268	−0.0742	7.79	−40285	−187424	+147138
	$TO2$	[69]	+0.2093	−0.0357	+0.0389	−3.60	+4803	−177323	+182127
	$TO3$	[466]	+0.0318	−0.0011	−0.0024	6.38	+217662	−473571	+691233
	$LO1$	[77i]	+0.2570	−0.0162	−0.0057	(0.052)	–	–	–
$LiVO_3$	$TO1$	[448i]	+0.0216	+0.0651	−0.0722	19.70	−200861	−980925	+780064
	$TO2$	[137i]	+0.2573	−0.0218	−0.0140	0.43	−18810	+56318	−75128
	$TO3$	[498]	+0.0262	−0.0194	+0.0168	4.71	+248701	−158808	+407510
	$LO1$	[138i]	+0.2536	−0.0118	−0.0240	(-0.008)	–	–	–
$NaVO_3$	$TO1$	[459i]	+0.0021	+0.0665	−0.0716	20.18	−210723	−1161238	+950515
	$TO2$	[159]	+0.1328	−0.0315	−0.0301	1.20	+25365	+14090	+11274
	$TO3$	[538]	+0.0033	−0.0173	+0.0167	4.67	+290176	−190507	+480683
	$LO1$	[154]	+0.1318	−0.0390	−0.0216	(−0.034)	–	–	–

associated to the $TO2$ mode, that is unstable only in $LiVO_3$, show a large motion of A atoms in the four systems. However, the A-cations displace in-phase with oxygens in $LiTaO_3$ and $LiNbO_3$ and in antiphase in $LiVO_3$ and $NaVO_3$; at the opposite, the B-cations displace in antiphase with oxygens in $LiTaO_3$ and $LiNbO_3$, producing a still large $\bar{Z}_{TO2}^*$, while, they displace in-phase with oxygens in $LiVO_3$ and $NaVO_3$, causing the vanishing $\bar{Z}_{TO2}^*$. $TO3$ modes are highly stable in all the four systems.

The eigendisplacements associated to the unstable $LO1$ mode show a dominant A atoms motion in antiphase with both B atoms and oxygens (A-O motion seems in-phase in $LiTaO_3$, but O contribution is quasi-negligible). Such A-site driven character already suggests the active role of the Li-cation in driving the LO instability.

In order to estimate the correlation between $LO1$ and the TO modes, we calculated the overlap matrix elements between the corresponding eigendisplacements as $\langle \eta^{LO1}|M|\eta^{TO}\rangle$ (projection of $LO1$ mode on the basis of the TO modes, as in Ref. [34]) where $M = M_k\delta_{kk'}$ with M_k the mass of atom k. The results, reported in Table V, show that $LO1$ eigendisplacements are mainly associated to the TO modes displaying dominant A-atoms motions. In particular, in $LiTaO_3$ and $LiNbO_3$, $LO1$ results from a mixing between $TO1$ and $TO2$, while it is mainly associated to $TO2$ in $LiVO_3$ and $NaVO_3$. It is thus important to emphasize that there is no one-to-one correspondence between $LO1$ and $TO1$ as considered by Li *et al.* in Ref. [9].

Moreover, in the aim of quantifying the balance between the dipole-dipole long-range interactions and the short-range interactions behind the above-discussed unstable modes, we

TABLE IV. Born effective charges (BEC) and ε_∞. The nominal valence charges of A, B, and O are +1, +5, and −2, respectively. Only the diagonal elements are reported, the complete tensor is given in Supplemental Material (see [21]).

	$LiTaO_3$			$LiNbO_3$		
Atom	Z_{xx}^*	Z_{yy}^*	Z_{zz}^*	Z_{xx}^*	Z_{yy}^*	Z_{zz}^*
A	1.14	1.14	1.11	1.15	1.15	1.10
B	7.67	7.67	8.33	8.33	8.33	9.19
O_1	−2.34	−3.85	−3.15	−2.47	−3.87	−3.43
O_2	−4.12	−1.75	−3.15	−4.54	−1.80	−3.43
O_3	−2.34	−3.53	−3.15	−2.50	−3.85	−3.43
	ε_∞^{xx}	ε_∞^{yy}	ε_∞^{zz}	ε_∞^{xx}	ε_∞^{yy}	ε_∞^{zz}
ε_∞	5.20	5.20	5.63	6.12	6.12	6.80
	$LiVO_3$			$NaVO_3$		
Atom	Z_{xx}^*	Z_{yy}^*	Z_{zz}^*	Z_{xx}^*	Z_{yy}^*	Z_{zz}^*
A	1.14	1.14	1.12	1.04	1.04	1.05
B	11.20	11.20	12.36	13.13	13.13	12.80
O_1	−3.11	−5.10	−4.50	−3.50	−6.00	−4.61
O_2	−6.10	−2.11	−4.50	−7.20	−2.30	−4.61
O_3	−3.11	−5.10	−4.50	−3.50	−6.00	−4.61
	ε_∞^{xx}	ε_∞^{yy}	ε_∞^{zz}	ε_∞^{xx}	ε_∞^{yy}	ε_∞^{zz}
ε_∞	13.10	13.10	14.40	15.61	15.61	14.53

TABLE V. Overlap matrix elements $\langle \eta^{LO}|M|\eta^{TO}\rangle (M = M_\kappa\delta_{\kappa\kappa'})$ between TO modes eigenvectors and $LO1$ mode in the $R\bar{3}c$ paraelectric phase.

	$LiTaO_3$ $LO1$	$LiNbO_3$ $LO1$	$LiVO_3$ $LO1$	$NaVO_3$ $LO1$
$TO1$	0.73	0.52	0.06	0.11
$TO2$	0.68	0.85	0.99	0.99
$TO3$	0.08	0.06	0.01	0.03

TABLE VI. On-site force constants (in Hartree/bohr^2) along the z-direction (zz) associated to different atoms in the $R\bar{3}c$ paraelectric phase.

		$LiTaO_3$			$LiNbO_3$			$LiVO_3$			$NaVO_3$		
		Tot	LR	SR	Tot	LR	SR	Tot	LR	SR	Tot	LR	SR
A	(zz)	+0.0008	+0.0340	−0.0331	+0.0003	+0.0319	−0.0316	−0.0020	+0.0219	−0.0239	+0.0211	+0.0125	+0.0085
B	(zz)	+0.3161	−0.4004	+0.7165	+0.2794	−0.4150	+0.6945	+0.1916	−0.4367	+0.6283	+0.1834	−0.5409	+0.7243
O	(zz)	+0.1273	−0.1054	+0.2328	+0.1111	−0.1095	+0.2207	+0.0985	−0.1170	+0.2156	+0.0812	−0.1640	+0.2452

decomposed the phonons frequencies into two contributions, i.e., $\omega^2 = \omega^2_{LR} + \omega^2_{SR}$, as discussed in Ref. [29].

From this decomposition reported in Table III, it is interesting to note that only $TO1$ instability in $LiTaO_3$ and $TO2$ one in $LiVO_3$ originate from a global destabilizing SR interactions ($\omega^2_{SR} < 0$), while, all the other instabilities originate from destabilizing LR interactions ($\omega^2_{LR} < 0$). Nevertheless, the fact that $LiNbO_3$ also hosts the LO instability without showing global unstable SR interactions, suggests that this is not the necessary condition for hyperFE, but rather, the specific destabilizing SR interatomic interactions associated to the Li motion (dominant Li motion in $LO1$ mode is a common feature in $LiTaO_3$, $LiNbO_3$, and $LiVO_3$, see above).

Accordingly, to shed light on the necessary conditions that make the A-site motion active in the destabilization of the LO mode, we examined distinct atomic interactions, through the analysis of the on-site and interatomic force constants calculated in the $R\bar{3}c$ paraelectric phase. Interestingly, we found that the (zz) component (out-of-plane direction) of the on-site force constant for Li is vanishingly small in $LiTaO_3$ and $LiNbO_3$ and turns out to be negative for $LiVO_3$ (see Table VI). In particular, we noticed a negative contribution, i.e., destabilizing, of the SR part for the three systems displaying the unstable LO mode. The other components of the Li on-site force constants and all those of Na, B, and O are large and positive.

The SR nature of the $LO1$ instability and the active role played by Li are also highlighted from the examination of the interatomic force constants reported in Table VII. The A_0-O_1 IFC (equivalent to the A_0-$O_{2,3}$), related to the interaction between the undercoordinated A atom and the out-of-plane oxygens toward which it tends to displace, is destabilizing with respect to both the LR and the SR forces (positive values) in $LiTaO_3$, $LiNbO_3$, and $LiVO_3$ systems. On one hand, the destabilizing LR dipole-dipole interaction contributes to the instability of the $TO1$ mode; on the other hand, the destabilizing SR interaction is responsible for the $LO1$ instability and the character of the associated eigendisplacement, dominated by Li motion. The destabilizing A_0-O_1 interaction confirms also the correlated Li-O motion reported in Ref. [35]. Noteworthy, the SR part of the A_0-O'_3 IFC, related to the interaction between A atom and in-plane oxygens, is also destabilizing along the z-direction, but not strong enough to overcome the stable LR part. In $NaVO_3$, in which the $LO1$ is stable, the scenario is indeed different: it is only the LR dipole-dipole interaction to be destabilizing and that drives the cooperative Na-O polar motion (SR part of A_0-O_1 and A_0-O'_3 IFCs is negative).

The interatomic force constants between the B atoms and the oxygens exhibit a destabilizing LR dipole-dipole interaction as standard ferroelectric perovskites [30,31]; the LR forces are destabilizing along the direction parallel to the B–O bonds. In particular, $LiVO_3$ and $NaVO_3$, characterized by dominant antiphase displacement of V and O atoms and giant mode effective charges (due to anomalous BEC on V and O atoms as discussed in previous paragraph), exhibit much more unstable $TO1$ mode than $LiTaO_3$ and $LiNbO_3$.

We finally noted negative interatomic force constants between near and next-near neighboring A and B atoms, meaning that the motion of A and/or B atoms along the A–B chain would be in-phase, propagating thus the polar distortions along this chain (i.e., along the trigonal axis) [32].

C. Effect of isotropic pressure

Ferroelectricity is known to be highly sensitive to external pressure; in particular, it was highlighted that, in the high-pressure ferroelectricity, a crucial role is played by SR interactions, which become destabilizing [36–38]. Based on that, it appeared necessary to explore the effect of isotropic pressure (isotropic compressive strain) on hyperferroelectricity, which is, as showed in the previous section, mainly driven by destabilizing SR forces on A atoms.

Interestingly, the $LO1$ instability increases as a function of pressure in $LiTaO_3$, $LiNbO_3$, and $LiVO_3$ [Figs. 3(a), 3(c) and 3(e)]; the opposite trend is observed in $NaVO_3$ [Fig. 3(g)]. The destabilizing SR forces acting on Li atoms are in fact strengthened by the isotropic compressive strain, as shown in Figs. 3(b), 3(d) and 3(f); in particular, we observe that the on-site force constants of Li atoms become more and more negative with increasing pressure, following the evolution of its SR part. At the opposite, pressure increases the stiffness of Na atoms in $NaVO_3$: the on-site force constant associated to Na becomes more and more positive, as shown in Fig. 3(h).

Noteworthy, the contribution of the $TO1$ mode to the $LO1$ mode in $LiTaO_3$, $LiNbO_3$, and $LiVO_3$ also increases with pressure, as clearly shown from the evolution of the overlap matrix illustrated in Figs. 4(d), 4(e) and 4(f). This is correlated to the increasing Li-displacement in the $TO1$-eigendisplacement [see Figs. 4(a), 4(b) and 4(c)] and is consistent with the fact that $LO1$ is associated to the TO modes exhibiting a large motion of the frustrated atom, as discussed in the previous section.

More interestingly, we observed that the $LO1$ mode effective charges also increase with pressure for the three Li-based compounds (see Table VIII); this is due to the increasing of the antiphase oxygens motion in the $LO1$ eigendisplacement. Therefore, since the mode effective charges are giving, by construction, an idea about the polarity of the mode, this result suggests that an external pressure could enhance the

TABLE VII. Interatomic force constants (in Hartree/bohr^2) between pairs of atoms along the local longitudinal bond direction (‖) and the Cartesian z-direction (zz). The long-range (LR) and short-range (SR) contributions to the IFCs are reported. Distances (dist. in Å) between the atomic pairs are also given. Positive IFC corresponds to destabilizing interaction, as discussed in Sec. III B.

		$LiTaO_3$			$LiNbO_3$			$LiVO_3$			$NaVO_3$		
Atoms		Tot	LR	SR	Tot	LR	SR	Tot	LR	SR	Tot	LR	SR
$A_0 - O_3'$	(‖)	−0.0150	+0.0144	−0.0295	−0.0150	+0.0124	−0.0274	−0.0161	+0.0068	−0.0229	−0.0077	+0.0034	−0.0111
	(zz)	−0.0049	−0.0116	+0.0066	−0.0047	−0.0103	+0.0056	−0.0030	−0.0065	+0.0034	−0.0022	−0.0037	+0.0015
	dist.	(1.97)			(1.96)			(1.96)			(2.39)		
$A_0 - O_1$	(‖)	+0.0057	+0.0044	+0.0013	+0.0055	+0.0037	+0.0017	+0.0047	+0.0027	+0.0020	+0.0007	+0.0025	−0.0018
	(zz)	+0.0012	+0.0001	+0.0011	+0.0013	−0.0002	+0.0014	+0.0013	−0.0003	+0.0016	−0.0011	+0.0001	−0.0013
	dist.	(2.79)			(2.79)			(2.61)			(2.62)		
$B_0 - O_1$	(‖)	−0.0573	+0.2994	−0.3568	−0.0418	+0.3021	−0.3439	+0.0119	+0.3136	−0.3017	+0.0334	+0.3709	−0.3379
	(zz)	−0.0250	+0.0726	−0.0976	−0.0174	+0.0750	−0.0924	+0.0052	+0.0779	−0.0727	+0.0105	+0.0969	−0.0865
	dist.	(1.97)			(1.98)			(1.85)			(1.85)		
$B_0 - O_3'$	(‖)	+0.0189	+0.0189	+0.0000	+0.0182	+0.0182	+0.0000	+0.0162	+0.0162	+0.0000	+0.0149	+0.0149	+0.0000
	(zz)	−0.0155	−0.0155	+0.0000	−0.0156	−0.0156	+0.0000	−0.0144	−0.0144	+0.0000	−0.0117	−0.0117	+0.0000
	dist	(3.75)			(3.75)			(3.63)			(3.99)		
$A_0 - A_0'$	(‖)	−0.0013	−0.0013	+0.0000	−0.0011	−0.0011	−0.0000	−0.0007	−0.0006	−0.0001	−0.0007	−0.0004	−0.0003
	(zz)	−0.0000	−0.0000	−0.0000	−0.0000	−0.0000	−0.0000	−0.0002	+0.0000	−0.0002	−0.0003	−0.0000	−0.0003
	dist	(3.75)			(3.76)			(3.56)			(3.69)		
$A_0 - A_1$	(‖)	−0.0002	−0.0002	−0.0000	−0.0002	−0.0002	+0.0000	−0.0001	−0.0001	+0.0000	−0.0000	−0.0000	+0.0000
	(zz)	−0.0002	−0.0002	+0.0000	−0.0002	−0.0002	+0.0000	−0.0001	−0.0001	+0.0000	−0.0000	−0.0000	+0.0000
	dist.	(6.82)			(6.82)			(6.35)			(6.39)		
$B_0 - B_0'$	(‖)	−0.0836	−0.0666	−0.0169	−0.0847	−0.0668	−0.0178	−0.0925	−0.0663	−0.0261	−0.0991	−0.0658	−0.0333
	(zz)	−0.0243	−0.0014	−0.0228	−0.0253	−0.0009	−0.0243	−0.0326	+0.0002	−0.0328	−0.0353	−0.0016	−0.0336
	dist.	(3.75)			(3.76)			(3.56)			(3.69)		
$B_0 - B_1$	(‖)	−0.0125	−0.0125	+0.0000	−0.0129	−0.0129	+0.0000	−0.0135	− 0.0135	+0.0000	−0.0118	−0.0118	0.0000
	(zz)	−0.0125	−0.0125	+0.0000	−0.0127	−0.0129	+0.0000	−0.0135	−0.0135	+0.0000	−0.0118	−0.0118	0.0000
	dist.	(6.82)			(6.82)			(6.35)			(6.39)		
$A_0 - B_0$	(‖)	−0.0134	−0.00134	+0.0000	−0.0124	−0.0124	+0.0000	−0.0097	−0.0097	0.0000	−0.0078	−0.0078	0.0000
	(zz)	−0.0134	−0.0134	+0.0000	−0.0124	−0.0124	+0.0000	−0.0097	−0.0097	+0.0000	−0.0078	−0.0078	+0.0000
	dist.	(3.41)			(3.41)			(3.17 int20)			(3.19)		
$O_1 - O_4$	(‖)	−0.0311	−0.0441	+0.0079	−0.0334	−0.0418	+0.0084	−0.0451	−0.0425	−0.0026	−0.0543	−0.0427	−0.0116
	(zz)	−0.0212	−0.0266	+0.0053	−0.0217	−0.0273	+0.0056	−0.0301	−0.0277	−0.0024	−0.0347	−0.0277	−0.0070
	dist.	(2.79)			(2.79)			(2.61)			(2.62)		

hyperferroelectric polarization. The polarization under open circuit conditions ($\mathbf{D} = 0$), not calculated in this work, is in fact found to be very small at 0GPa (see Refs. [1,7,9]).

IV. DISCUSSION

$LiTaO_3$, $LiNbO_3$, $LiVO_3$, and $NaVO_3$ compounds all exhibit polar instabilities; in particular, the unstable $TO1$ modes in $LiTaO_3$, $LiNbO_3$, and the $TO2$ one in $LiVO_3$ are characterized by dominant antiphase Li-O displacements (Table III). The A-cation in these ABO_3-$LiNbO_3$-type systems, experiences, in fact, an electrostatic frustration due to its undercoordination in the $R\bar{3}c$ paraelectric phase [8]: the off-centering of Li from its central position in the O-triangle toward the three out-of-plane oxygens (Fig. 2) optimizes Li-coordination from III, in the paraelectric $R\bar{3}c$ phase, to VI in the ferroelectric $R3c$ phase.

The instability of the polar $LO1$ mode is ascribed, in one hand, to this frustration, as the $LO1$ mode is mainly driven by the A-site motion and, on the other hand, to the small size of the frustrated cation. Here, the $LO1$ mode is in fact unstable only in the Li-based compounds, where Li has much smaller size than Na (0.76 versus 1.02 Å, respectively, for six-coordinated cations [39]). Moreover, by analyzing the on-site (Table VI) and the interatomic (Table VII) force constants, we found out that the $LO1$ instability is driven by short-range interactions: $LiTaO_3$, $LiNbO_3$, and $LiVO_3$ exhibit destabilizing Li-O interactions with dominant contribution coming from SR forces; this leads to vanishingly small or even negative Li on-site force constants, that is not observed in the case of $NaVO_3$.

Our findings on ABO_3-$LiNbO_3$-type systems are also confirmed in the prototype hyperFEs, the ABC-hexagonal systems [1]. In the ABC-hexagonal systems, it is the small B cation, undercoordinated in the paraelectric $P6_3/mmc$ phase, to experience a structural frustration [see Fig. 5(a)]: as for Li in the $LiNbO_3$-type systems, the B cation sits a the center of a triangle formed by three near-neighbor C-anions;

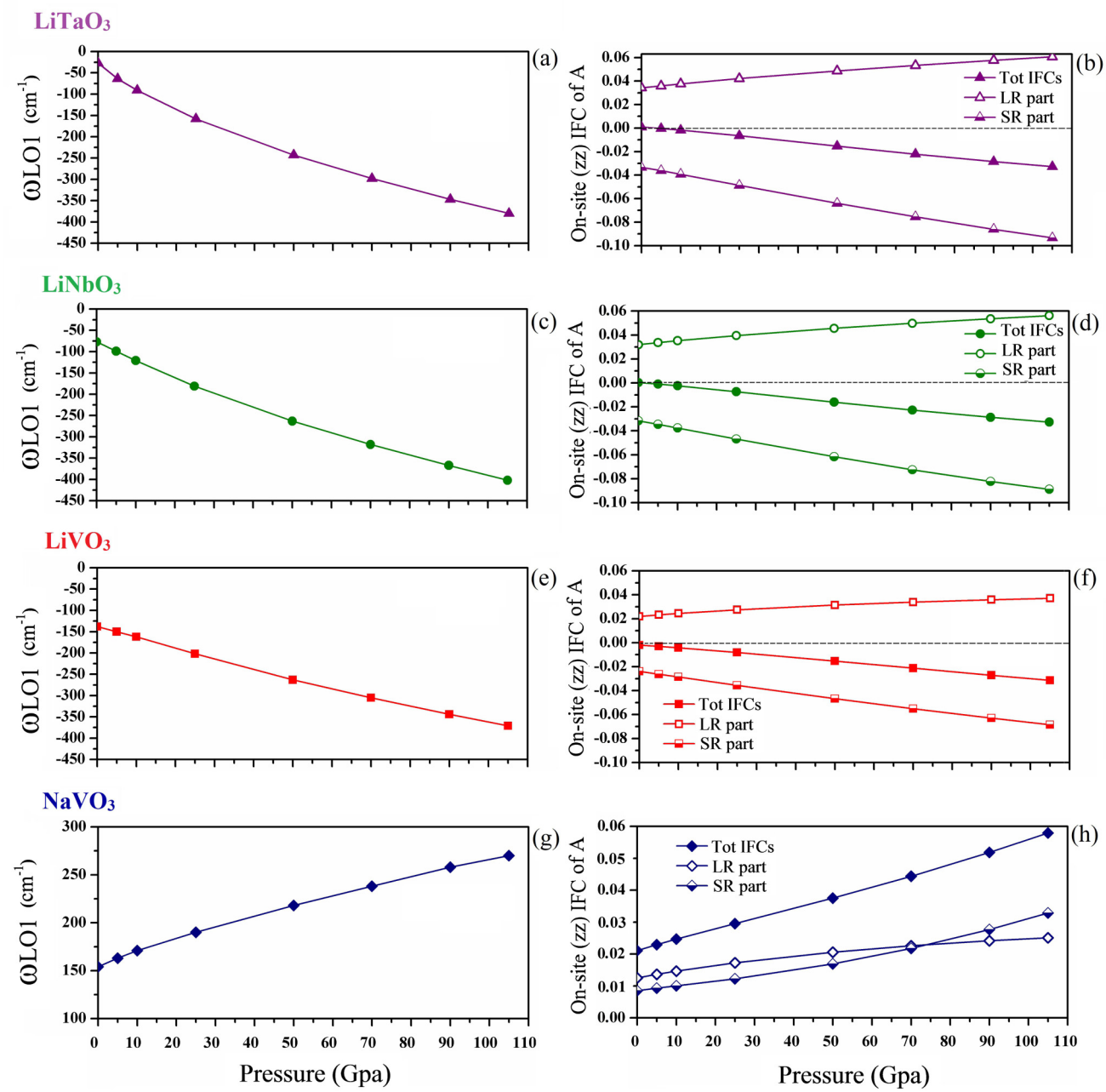

FIG. 3. (a), (c), (e), and (g) Evolution of $LO1$ mode frequency with pressure. (b), (d), (f), and (h) Evolution of the total (zz) on-site IFC of A atoms with pressure, together with its LR and SR parts.

its off-centering towards the apical C-anion (along the z-direction) improves its coordination from III, in the paraelectric $P6_3/mmc$ phase, to IV, in the ferroelectric $P6_3mc$ phase (see Fig. 5). By exploring the on-site and B-C interatomic force constants in LiBeSb, LiZnAs, LiZnP, and NaMgP, taken as representative examples, we found out that the $LO1$ instability occurs in the compounds which exhibit some dominant destabilizing SR interactions, like LiBeSb and LiZnAs. In these systems, the zz component of the on-site force constant of the frustrated B-cation is negative and the B-C_0 interaction is positive (Table IX), in line with what we argued for the $LiNbO_3$-type systems.

We also suggested the possible enhancement of hyperferroelectricity in $LiNbO_3$-type compounds by applying an external isotropic pressure. Indeed, pressure strengthens the short-range forces, as observed from the trend of the zz- component of the on-site force constants of Li in $LiTaO_3$, $LiNbO_3$, and $LiVO_3$, which becomes more and more negative; in turn, this produces further softening of the $LO1$ frequency, which becomes, monotonically, more and more unstable (Fig. 3). Interestingly, the Callen mode effective charge associated to the $LO1$ mode increases with pressure (Table VIII), suggesting thus a possible increase in the hyperferroelectric polarization.

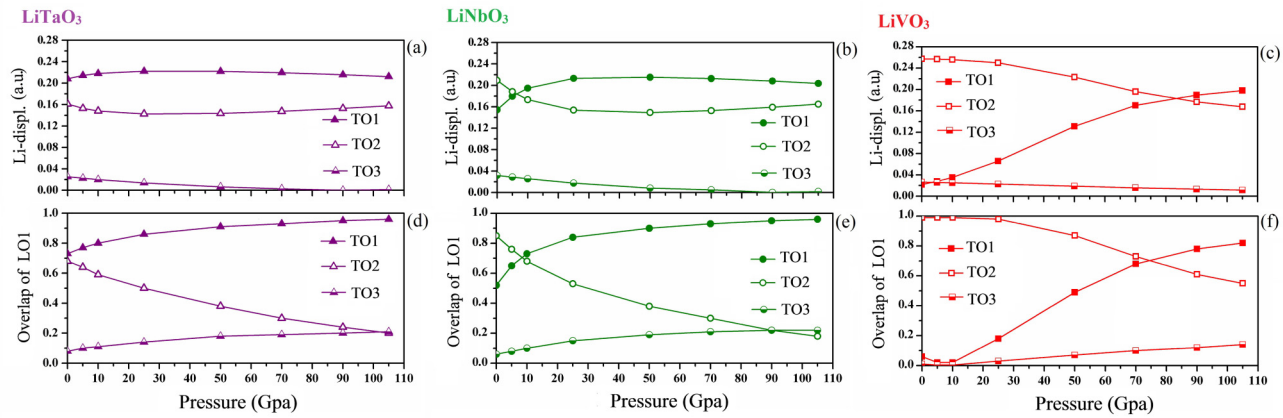

FIG. 4. (a)–(c) Evolution of Li displacement (in atomic unit) with pressure in $TO1$, $TO2$, and $TO3$ polar modes. (d)–(f) Evolution with pressure of the overlap of the $LO1$ mode with $TO1$, $TO2$ and $TO3$ modes.

Finally, it is also noteworthy to mention that the current literature is considering that the unstable LO mode arises from a small LO-TO splitting [1,9]. This notion is, however, not conclusive since one-to-one correspondence between TO and LO modes does not always occur, as in the discussed cases of ABO_3-$LiNbO_3$-type systems. The calculation of the overlap matrix (Table V) showed, in fact, that the unstable $LO1$ mode totally corresponds to one unstable TO mode only in $LiVO_3$ (i.e., $TO2$); in $LiTaO_3$ and $LiNbO_3$, the unstable $LO1$ mode is correlated to two TO modes (the unstable $TO1$ and the stable $TO2$). Moreover, the overlap matrix also revealed that the TO modes contributing to the LO one are those characterized by large motion of Li atoms, consistently with the Li-driven character of the structural instability. Worthy of note that a possible mixing of TO modes was already mentioned in Ref. [40] to explain the LO instabilities found in the candidate hyperFE $SrNb_6O_{16}$ despite its large effective charges; nevertheless, the authors did not argue about this in detail.

TABLE VIII. Effect of increasing pressure on $LO1$ mode frequency, on $LO1$ eigenvectors along the z-direction and on longitudinal mode effective charges ($\bar{Z}^{*L}_{LO1}$).

P(Gpa)	ω_{LO1}	A	B	$O_{1/2/3}$	$\bar{Z}^{*L}_{LO1}$
$LiTaO_3$					
0	[28i]	+0.2594	−0.0105	+0.0021	0.077
5	[64i]	+0.2597	−0.0101	+0.0006	0.093
10	[91i]	+0.2598	−0.0096	−0.0010	0.110
25	[158i]	+0.2591	−0.0083	−0.0061	0.156
50	[243i]	+0.2549	−0.0059	−0.0145	0.224
70	[299i]	+0.2491	−0.0040	−0.0207	0.270
90	[347i]	+0.2415	−0.0022	−0.0265	0.310
105	[381i]	+0.2347	−0.0008	−0.0306	0.336
$LiNbO_3$					
0	[77i]	+0.2570	−0.0162	−0.0057	0.053
5	[99i]	+0.2571	−0.0155	−0.0072	0.068
10	[121i]	+0.2570	−0.0147	−0.0087	0.084
25	[181i]	+0.2556	−0.0123	−0.0132	0.127
50	[263i]	+0.2501	−0.0081	−0.0205	0.192
70	[318i]	+0.2429	−0.0046	−0.0262	0.236
90	[368i]	+0.2334	−0.0011	−0.0315	0.274
105	[402i]	+0.2248	+0.0014	−0.0353	0.299
$LiVO_3$					
0	[138i]	+0.2559	−0.0258	−0.0096	−0.008
5	[150i]	+0.2562	−0.0250	−0.0105	0.001
10	[162i]	+0.2565	−0.0243	−0.0113	0.010
25	[202i]	+0.2570	−0.0221	−0.0136	0.033
50	[263i]	+0.2569	−0.0188	−0.0172	0.064
70	[305i]	+0.2561	−0.0162	−0.0198	0.085
90	[344i]	+0.2549	−0.0137	−0.0223	0.104
105	[371i]	+0.2536	−0.0119	−0.0241	0.116

V. CONCLUSION

In this paper we investigated the dynamical properties of $LiTaO_3$, $LiNbO_3$, $LiVO_3$, and $NaVO_3$ compounds by means of first-principles calculations, revealing microscopic mechanisms of general validity behind hyperferroelectricity; we provided, in fact, a confirmation also for the ABC-hexagonal systems. In particular, we showed that, beyond the small LO-TO splitting claimed in literature, the LO mode instability is driven by destabilizing short-range forces acting on the small sized cations at the A-site of the ABO_3-$LiNbO_3$-type systems and at the B-site of the ABC-hexagonal ones, which experience an electrostatic frustration caused by their undercoordination in their respective centrosymmetric paraelectric

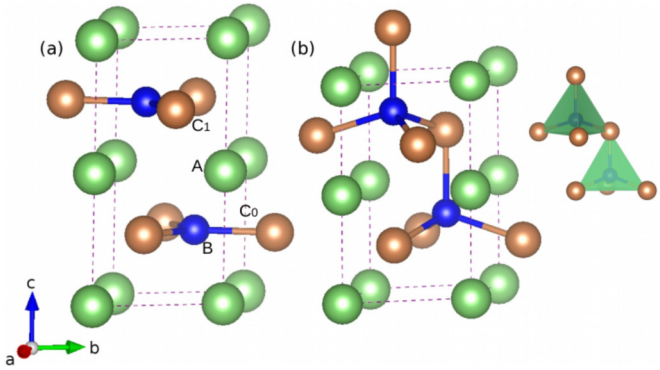

FIG. 5. ABC-hexagonal cell in the paraelectric $P6_3/mmc$ and polar $P6_3mc$(186) phases.

TABLE IX. On-site and interatomic force constants in (Hartree/bohr^2) related to different atoms of the hexagonal ABC systems calculated in the $P6_3/mmc$ (194) paraelectric phase.

		LiBeSb (LO = 16i, TO$_1$ = 126i)			LiZnP (LO = 82, TO$_1$ = 82i)			LiZnAs (LO = 36i, TO$_1$ = 83i)			NaMgP (LO = 155, TO$_1$ = 113i)		
		Tot	LR	SR	Tot	LR	SR	Tot	LR	SR	Tot	LR	SR
A	(zz)	+0.0178	+0.0006	+0.0172	+0.0172	−0.0010	+0.0182	+0.0149	−0.0011	+0.0160	+0.0297	+0.0013	+0.0284
B	(zz)	−0.0011	+0.0045	−0.0056	+0.0022	+0.0100	−0.0078	−0.0042	+0.0082	−0.0124	+0.0023	+0.0066	−0.0043
C	(zz)	+0.0158	+0.0047	+0.0111	+0.0061	+0.0059	+0.0001	+0.0009	+0.0043	−0.0034	+0.0103	+0.0087	+0.0016
$B-C_0$	(zz)	+0.0003	−0.0025	+0.0029	+0.0004	−0.0040	+0.0045	+0.0022	−0.0032	+0.0054	−0.0009	−0.0050	+0.0041
	dist.	(2.36)			(2.31)			(2.40)			(2.53)		
$B-C_1$	(zz)	+0.0019	+0.0018	+0.0001	+0.0016	+0.0018	−0.0002	+0.0013	+0.0013	−0.0000	+0.0046	+0.0048	−0.0002
	dist.	(3.87)			(3.64)			(3.73)			(3.63)		

phases. The signature of such SR-driven *LO* instability is a vanishingly small or negative on-site force constant associated to the frustrated cation, which reflect its tendency to displace, combined to destabilizing cation-anion interactions; both effects associated to destabilizing SR forces. Moreover, we also predicted a possible enhancement of hyperferroelectricity upon external isotropic pressure, which can be suitable for technological applications.

ACKNOWLEDGMENTS

The authors acknowledge Ph. Ghosez from University of Liège for useful discussions. Computational resources are provided from CDTA cloud platform. M.K. and H.D. acknowledge support from Algerian-WBI bilateral cooperative project. D.A. is grateful to S. Picozzi (CNR-SPIN) for the provided time to work on this paper.

[1] K. F. Garrity, K. M. Rabe, and D. Vanderbilt, Phys. Rev. Lett. **112**, 127601 (2014).
[2] W. Zhong, R. D. King-Smith, and D. Vanderbilt, Phys. Rev. Lett. **72**, 3618 (1994).
[3] H. Fu, J. Appl. Phys. **116**, 164104 (2014).
[4] W. Luo, K. Xu, and H. Xiang, Phys. Rev. B **96**, 235415 (2017).
[5] D. Du, P. J. Strohbeen, H. Paik, C. Zhang, K. T. Genser, K. M. Rabe, P. M. Voyles, D. G. Schlom, and J. K. Kawasaki, J. Vac. Sci. Technol B **38**, 022208 (2020).
[6] D. Di Sante, P. Barone, A. Stroppa, K. F. Garrity, D. Vanderbilt, and S. Picozzi, Phys. Rev. Lett. **117**, 076401 (2016).
[7] G. Roma, A. Marronnier, and J. Even, Phys. Rev. Materials **4**, 092402(R) (2020).
[8] H. J. Xiang, Phys. Rev. B **90**, 094108 (2014).
[9] P. Li, X. Ren, G.-C. Guo, and L. He, Sci. Rep. **6**, 34085 (2016).
[10] R. E. Cohen and H. Krakauer, Phys. Rev. B **42**, 6416 (1990).
[11] K. M. Rabe, M. Dawber, C. Lichtensteiger, C. H. Ahn, and J.-M. Triscone, Modern physics of ferroelectrics: Essential background. physics of ferroelectrics, in *Physics of Ferroelectrics* (Springer-Verlag, Berlin, 2007), Chap. 7, pp. 1–30.
[12] J. W. Bennett, K. F. Garrity, K. M. Rabe, and D. Vanderbilt, Phys. Rev. Lett. **109**, 167602 (2012).
[13] P. Hohenberg and W. Kohn, Phys. Rev. **136**, B864 (1964).
[14] W. Kohn and L. J. Sham, Phys. Rev. **140**, A1133 (1965).
[15] X. Gonze,, B. Amadon, P.-M. Anglade, J.-M. Beuken, F. Bottin, P. Boulanger, F. Bruneval, D. Caliste, R. Caracas, T. Deutsch, L. Genovese, P. Ghosez, M. Giantomassi, S. Goedecker, D. Hamann, P. Hermet, F. Jollet, G. Jomard, S. Leroux, M. Mancini, S. Mazevet, M. Oliveira, G. Onida, Y. Pouillon, T. Rangel, G.-M. Rignanese, D. Sangalli, R. Shaltaf, M. Torrent, M. Verstraete, G. Zerah, and J. Zwanziger, Comput. Phys. Commun. **180**, 2582 (2009).
[16] J. P. Perdew, A. Ruzsinszky, G. I. Csonka, O. A. Vydrov, G. E. Scuseria, L. A. Constantin, X. Zhou, and K. Burke, Phys. Rev. Lett. **100**, 136406 (2008).
[17] M. van Setten, M. Giantomassi, E. Bousquet, M. Verstraete, D. Hamann, X. Gonze, and G.-M. Rignanese, Comput. Phys. Commun. **226**, 39 (2018).
[18] H. J. Monkhorst and J. D. Pack, Phys. Rev. B **13**, 5188 (1976).
[19] S. Baroni, S. de Gironcoli, A. Dal Corso, and P. Giannozzi, Rev. Mod. Phys. **73**, 515 (2001).
[20] X. Gonze and C. Lee, Phys. Rev. B **55**, 10355 (1997).
[21] See Supplemental Material at http://link.aps.org/supplemental/10.1103/PhysRevB.103.014116 for cell parameters and atomic coordinates of $LiTaO_3$, $LiNbO_3$, $LiVO_3$, and $NaVO_3$, the complete Born effective charges matrix and the eigendisplacements in atomic unit.
[22] M. Veithen and P. Ghosez, Phys. Rev. B **65**, 214302 (2002).
[23] K. Parlinski, Z. Q. Li, and Y. Kawazoe, Phys. Rev. B **61**, 272 (2000).
[24] K. Toyoura, M. Ohta, A. Nakamura, and K. Matsunaga, J. Appl. Phys. **118**, 064103 (2015).
[25] K. M. Rabe and J. D. Joannopoulos, Phys. Rev. B **36**, 6631 (1987).
[26] R. D. King-Smith and D. Vanderbilt, Phys. Rev. B **49**, 5828 (1994).
[27] W. Zhong, D. Vanderbilt, and K. M. Rabe, Phys. Rev. B **52**, 6301 (1995).
[28] W. Cochran, Phys. Rev. Lett. **3**, 412 (1959).
[29] P. Ghosez, X. Gonze, and J.-P. Michenaud, Europhys. Lett. **33**, 713 (1996).
[30] P. Ghosez, E. Cockayne, U. V. Waghmare, and K. M. Rabe, Phys. Rev. B **60**, 836 (1999).

[31] D. Amoroso, A. Cano, and P. Ghosez, Phys. Rev. B **97**, 174108 (2018).
[32] P. Ghosez, J.-P. Michenaud, and X. Gonze, Phys. Rev. B **58**, 6224 (1998).
[33] H. B. Callen, Phys. Rev. **76**, 1394 (1949).
[34] H. Djani, E. Bousquet, A. Kellou, and P. Ghosez, Phys. Rev. B **86**, 054107 (2012).
[35] I. Inbar and R. E. Cohen, Ferroelectrics **194**, 83 (1997).
[36] G. A. Samara, T. Sakudo, and K. Yoshimitsu, Phys. Rev. Lett. **35**, 1767 (1975).
[37] I. A. Kornev, L. Bellaiche, P. Bouvier, P.-E. Janolin, B. Dkhil, and J. Kreisel, Phys. Rev. Lett. **95**, 196804 (2005).
[38] E. Bousquet and P. Ghosez, Phys. Rev. B **74**, 180101(R) (2006).
[39] R. Shannon and C. Calvo, Can. J. Chem. **51**, 265 (1973).
[40] K. F. Garrity, Phys. Rev. B **97**, 024115 (2018).